Design optimization for x-ray telescopes

Timo T. Saha and William W. Zhang

NASA/Goddard Space Flight Center, Greenbelt, MD 20771

ABSTRACT

The capability of future X-ray telescopes depends on the quality of their Point Spread Function (PSF) and the size of their field of view. Traditional designs, such as Wolter, and Wolter-Schwarzschild telescopes are stigmatic on the optical axis but their PSF degrades rapidly off-axis. At the optimal focal surface, their PSFs can be significantly improved. We present a simple optimization process for Wolter (W), Wolter-Schwarzschild (WS) and Hyperboloid-Hyperboloid (HH) telescopes that substantially improves the off-axis PSF for either narrow or wide field of view applications. In this paper, we will compare the optical performance of conventional and optimized W-, WS-, and HH-telescopes for a wide range of telescope diameters that can be used to build up future x-ray telescopes.

Keywords: Optical design, x-ray optics, x-ray mirrors, wide-field x-ray telescopes

1. INTRODUCTION

Advances in structural design [1], mirror fabrication technologies [2, 3] and development of assembly and alignment techniques [4] has led to significant improvements in the resolution of x-ray telescopes. Conventional x-ray telescopes suffer from large off-axis aberrations and full benefits of these improvements cannot be taken advantage of. Wolter x-ray telescope [5, 6] consists of paraboloidal primary mirror and hyperboloidal secondary mirror. Secondary mirror is coaxial and confocal with the primary mirror and, therefore, the telescope forms stigmatic on-axis image. Off-axis image quality degrades rapidly due to large system aberrations. Main aberrations of the designs are field curvature and coma. Field curvature is caused by large Optical Path Differences (OPD) between sets of rays emanating for opposite sides of the entrance aperture. Also, off-axis rays at the entrance aperture starting from outer radial zones are focused at different axial locations than off-axis rays starting from inner radial zones. At the Gaussian focal plane off-axis images have toroidal shapes. Near on-axis coma starts dominating and toroidal image breaks down to two toroidal circles partially overlapping each other. Typically smaller radial heights and longer axial lengths of the mirrors increase the field curvature and image size at the Gaussian focal plane and at the optimal focal surface.

Wolter-Schwarzschild (WS) telescopes [7] satisfy Abbe's sine condition and, therefore, coma aberration is eliminated from the design. Field curvatures of WS-telescopes are still comparable to field curvatures of W-telescopes. WS-telescopes are stigmatic on-axis and provide significantly better resolution for narrow field of views. Surface equations of W-telescope and WS-telescope can be combined into a single set of equations providing simple basic platform for design and ray trace analysis [8].

Hyperboloid-Hyperboloid (HH) x-ray telescopes were originally developed for solar physics applications by Thompson and Harvey [9]. Optimization methods of commercial ray trace codes were used to balance the resolution across the field of view. HH-telescopes are no longer stigmatic and the optimization process minimizes coma aberrations in the balancing process. Magnitude of the field curvature of HH-telescopes remains close to the field curvature of W-telescopes and WS-telescopes.

Polynomial x-ray telescopes were introduced by Burrows [10] for wide field of view applications. Optimization methods of commercial ray trace programs were used to balance aberrations of a two mirror telescope across a 1-degree field of view. General polynomials were used to describe the primary mirror and the secondary mirror. Several other authors [11, 12, 13] have studied polynomial telescopes and developed nested telescope designs based on this concept.

Different optimization method is presented in this paper. Development is based on an addition of small axial polynomial terms to baseline W-telescopes or WS-telescopes. Basic version of this approach was implemented in the design of telescope for Survey and Time Domain Advanced Research Explorer (STARX) [14, 15], where axial

second order sags were added to balance the image size of the telescope across the field of view. In this study, additional higher order polynomial terms on the mirror surfaces are optimized for a field point at the edge of the field of view. Optimization can be done for narrow or wide field of view applications by selecting magnitude of polynomial terms appropriately. For narrow field of view applications polynomial terms have to be selected so that the aberrations generated by added primary and secondary polynomial terms cancel each other, thus, providing near perfect on-axis images.

2. SURFACE EQUATIONS AND DESIGN OPTIMIZATION

Mirrors of x-ray W-telescopes can be described by unique sets of equations convenient for grazing incidence configuration. Surfaces of primary mirror and secondary mirror can be described in polar coordinates using equations:

$$\rho = R_1/(1-\cos(\Theta)) \tag{1}$$

for the primary mirror and

$$r = R_2/(\varepsilon\cos(\Theta)-1) \;\; or \;\; q = R_2/(1-\varepsilon\cos(\alpha)) \tag{2}$$

for the secondary mirror. Surfaces and coordinate variables are shown in Figure 1. Parameters R_1 and R_2 in the equations are the vertex radii of curvatures of the primary and secondary mirror, respectively. Parameter ε is the eccentricity of the secondary mirrors.

In Cartesian coordinates (h_b, z_b) the primary and secondary mirrors of x-ray W- or HH-telescopes can be described using a following equation:

$$h_b = \sqrt{h_{b0}^2 + 2Kz_b - Pz_b{}^2}. \tag{3}$$

The parameter h_{b0} is the radial height of the mirrors at the axial mid-point of the surface, K is related to the slope of the surface and P is related to the eccentricity of the surface ($P=1-\varepsilon^2$). If the parameter P is equal to zero, the surface is parabolic. If P is nonzero the surface can be either hyperbolic or elliptic. This set of equations was implemented in the OSAC ray trace program [16]. Optimization of hyperboloid-hyperboloid telescopes is based on the application of Eq. (3).

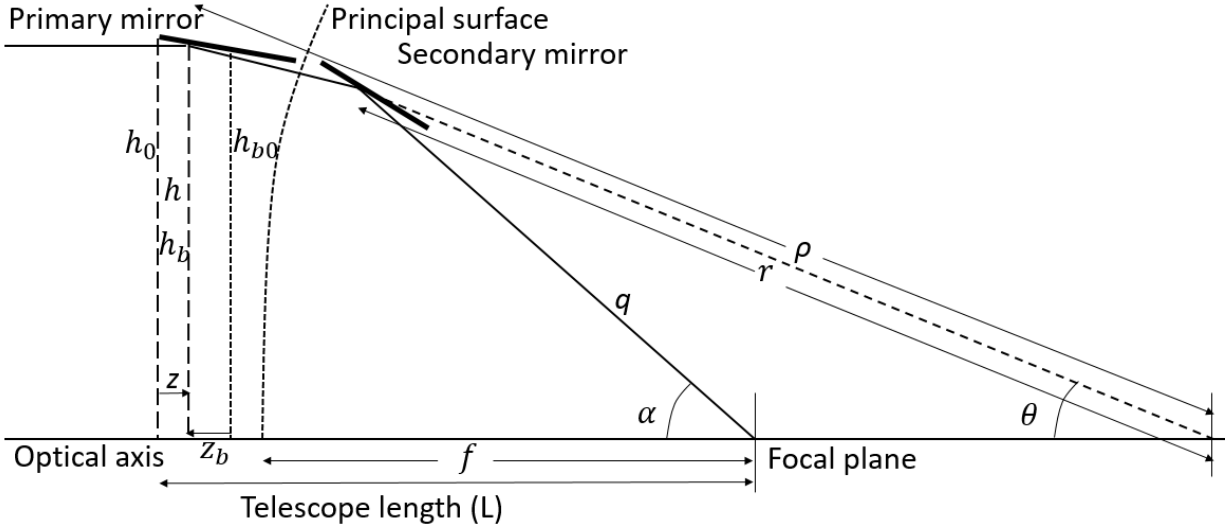

Figure 1. Cross-section of a type 1 x-ray telescope showing primary mirror, secondary mirror, coordinate systems, parameters, and variables used in the surface equations.

A third set of equations used are for W-and WS-telescopes. This set combines the equations of W-telescopes and WS-telescopes and can be conveniently used in the design and ray trace analyses. Primary and secondary mirror

equations are a set of parametric equations relating system parameters to the variables of the telescopes. The primary and secondary mirrors are described by the following equations:

$$z = L + fk - \frac{h^2}{4fk} + C_z \frac{|k-(1-nkt^2)|^{\frac{1-2nk}{1-nk}}}{|1+nt^2|^2} \quad (4)$$

$$\frac{1+t^2}{q} = \frac{t^2}{fk} - \frac{1}{C_z k^2} |k-(1-nk)t^2|^{\frac{1}{1-nk}} \quad (5)$$

where n, f, k, L, and C_z are surface parameters [8, 14] and variable t is related to the radial height (h) of the primary mirror through relation:

$$h = 2ft/(1+nt^2). \quad (6)$$

Selecting n=0 reduces Eqs. (4), (5), and (6) to the equations for paraboloid and hyperboloid (Eqs. (1), (2), or Eq. (3)). If n=1, the surfaces describe WS-telescopes.

In the Optical Surface Analysis Code (OSAC) [16, 17] axial surface deformations (Δh) are described by a set of Legendre polynomials as a function of axial coordinate z_b:

$$\Delta h = \sum_{i=0}^{n} A_i LEGENDRE_i\,(2z_b/L_z), \quad (7)$$

where $LEGENDRE_i$ is the Legendre polynomial of order i, A_i is its coefficient, and L_z is the axial length of the mirror. The origin of the axial coordinate z_b is located at the axial center of the primary or secondary mirror.

Surface equations (4), (5), and (6) are used to design and evaluate optimized W-telescopes and WS-telescopes. Optimized telescopes are then a combination of base W-telescope or WS-telescope described by Eqs. (4) and (5) or Eq. (3), and additional second, third, and fourth order axial Legendre polynomials described by Eq. (7).

Telescope optimization process for HH-telescopes, optimized W-telescopes, and WS-telescopes is demonstrated on the STARX telescope [14, 15]. Nested mirror pairs of the STARX telescope are designed so that the focal lengths of individual telescopes are 5000 mm. Primary-secondary intersection points of the individual telescopes are placed on the common spherical principal surface of the nested telescope. Radial heights of the nested mirrors range approximately from 250mm to 650 mm and axial lengths of the primary mirrors and secondary mirrors are 100 mm. There is a constant 5 mm gap between primary and secondary mirrors.

3. OPTIMIZED HYPERBOLOID-HYPERBOLOID TELESCOPES

W-telescopes consisting of paraboidal primary mirror and hyperboloidal secondary mirror is a special case of more general HH-telescopes. Hyperboloids can be approximated by expanding the surface equation (3) in a specific manner. Equation of a paraboloid has only two first terms of Eq. (3). If we now expand the third term in Eq. (3), we get an approximation for the hyperboloid:

$$h_b = \sqrt{h_{bo}^2 + 2Kz_b} - \frac{Pz_b{}^2}{2h_{bo}^2} + higher\ order\ z_b - terms \quad (8)$$

In other words, a grazing incidence hyperboloid can be approximately described by a paraboloid with a small second order term added on the top of the base paraboloid. Residual higher order terms are small since the parameter P in x-ray telescopes is very small and typically radial height parameter h_{b0} is larger than the axial coordinate z_b.

2.1. Optimization process of HH-telescopes

The optimization process of HH-telescopes starts with a base W-telescope. In the first step we add an equal but opposite amount of eccentricity to the primary mirror and secondary mirror. This process does not significantly change the on-axis aberrations or images because the added second order axial sag of the primary roughly cancels the added second order axial sag of the secondary. At the edge of the field of view Root-Mean-Square image diameters (RMSD) are calculated for a range of eccentricities till minimum diameter is found. In the optimization process optimal axial location of the off-axis images is also found. Figure 2 plots the axial location of the optimal

focus as a function of radial heights of the mirror pairs of STARX telescope at the edge of the 0.5-degree field of view. The plot shows that, at the edge of the field of view, the optimal focus moves farther away from the Gaussian focal plane when the radial heights of the mirror pairs are getting smaller. This is one of the largest aberrations in x-ray telescopes.

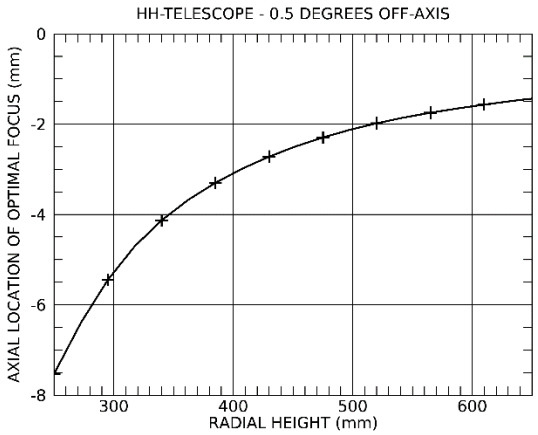

Figure 2. Axial location of optimal focus of HH-telescopes in radial height range from 250 mm to 650 mm.

Figure 3A shows Half Power Diameter (HPD) as a function of radial heights at the edge of 0.5-degree field of view for base W-telescopes and optimized HH-telescopes. HPDs are calculated at the optimal focal surface. Black curve represents the HPD of the W-telescopes at the edge of 0.5 degree field of view. Red curve is for optimized HH-telescopes where optimization is accomplished by varying primary and secondary eccentricities an equal but opposite amount

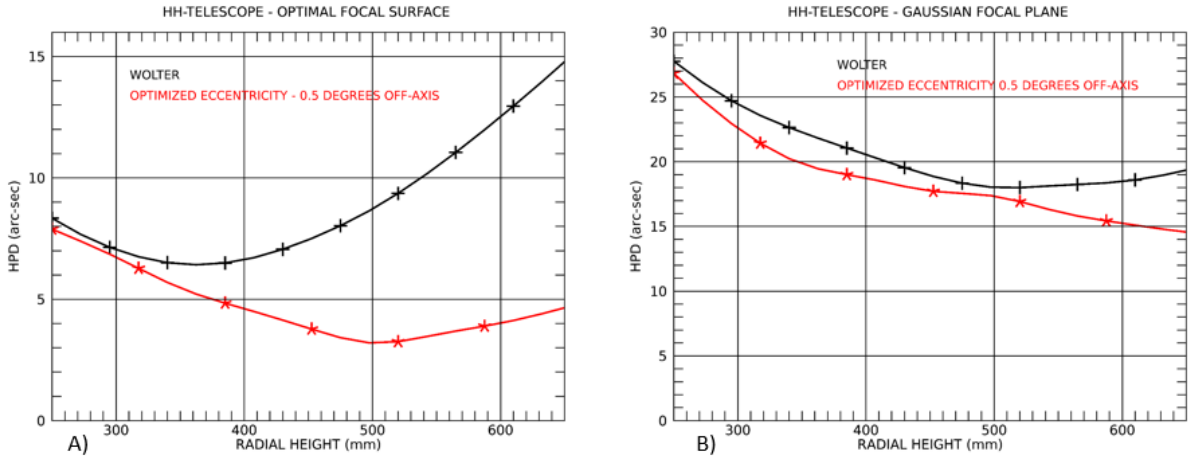

Figure 3. HPD plotted in radial height range from 250 mm to 650 mm for W-telescopes and optimized HH-telescopes at the edge of 0.5 degree field of view and calculated at the optimal focal surface (A) and at the Gaussian focal plane (B).

till optimum RMSD is found at the edge of 0.5-degree field of view. On-axis HPD or RMSD remains negligible through the optimization process. At the Gaussian focal plane the improvement is not as impressive. Figure 3B shows the HPDs calculated at the Gaussian focal plane for the HH-telescopes. Curvature of the optimal focal surface is the dominating aberration and nullifies the advantages seen at the optimal focal surface.

In wide field of view telescopes the optimization process is designed to yield the same on-axis and off-axis image diameter. Figure 4 shows the HPD at the optimal focal surface locations as a function of radial heights from 250 mm to 650 mm for on-axis image location and 0.5-degree off-axis image location. Under these conditions, radial height of the telescope of about 450 mm provides

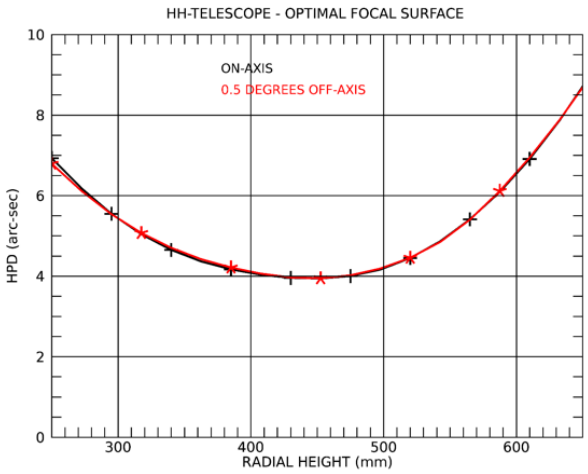

Figure 4. HPD shown in 250 mm – 650 mm radial height range for designs which have equal on-axis (+) and off-axis (*) HPDs.

the best image quality of about 4.0 arc-sec. HPDs start increasing towards smaller or larger radial heights.

Figure 3 and 4 demonstrates that at the optimal focal surface HH-telescopes designed for wide field of view applications (equal on-axis and off-axis HPD) or narrow field of view applications (negligible on-axis HPD) offer significant improvements in wide range of radial heights over conventional W-telescopes. In the optimized HH-telescopes added eccentricities reshape the coma of W-telescopes. Off-axis images become more symmetric. This process significantly improves RMSDs and HPDs because the centroids of the images are now located closer to the center of the image. Note that forcing equal on-axis and off-axis HPDs does not necessarily lead to optimum telescope designs across the radial height range. Based on Figure 3 and 4, HH-telescopes designed for optimal on-axis and off-axis HPDs outperform the telescopes designed for equal on-axis and off-axis HPDs in 420 mm – 650 mm radial range.

Image centroid coordinates of individual telescopes in the nested telescope systems are an important factor in determining off-axis response of a nested telescope systems. Figure 5 plots the deviation of radial image centroids at 0.5-degrees off-axis from the mean centroids of individual HH-telescopes in radial height range from 250 mm to 650 mm. The centroids are shown at Gaussian focal plane and also at the optimal focal surface. Ranges of mean radial centroids could adversely affect the resolution of nested telescopes and even become dominating factor in the resolution requirements.

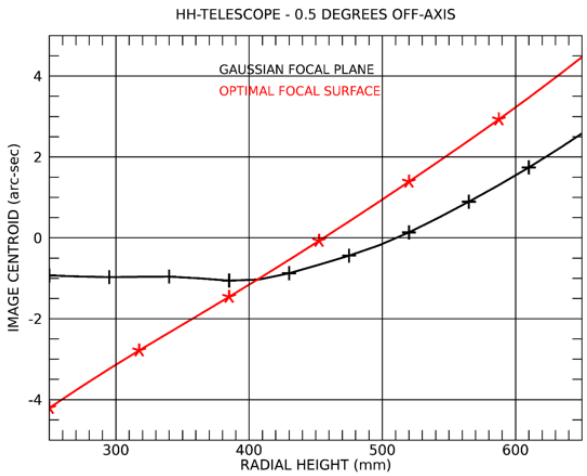

Figure 5. Deviation of image centroid coordinates from mean centroid plotted at the optimal focal surface (+) and at the Gaussian focal plane (*).

3. OPTIMIZED WOLTER AND WOLTER-SCHWARZSCHILD TELESCOPES

In the optimization method axial second order, third order, and fourth order Legendre polynomials shown in Eq. (7) are added to the base surfaces of W-telescopes and WS-telescopes given by Eq. (4) and Eq. (5).

Adding equal but opposite amounts of axial even order polynomials to the primary mirrors and secondary mirrors adds negligible amount of aberrations to on-axis images. This is because a collimated on-axis set of rays that hit the front section of the primary mirror in type 1 W- and WS-telescopes are intersecting the secondary mirror closer to the back-section of the secondary mirror. In these locations the slopes of the added even order polynomials approximately cancel causing very small deviations in the ray locations at the image plane. Similarly, inserting equal amounts of axial odd order polynomials to the mirrors causes only negligible additional image defects at the focal plane.

The optimization method is similar to the optimization process developed for the HH-telescopes. First, coefficients of added second order Legendre polynomials are optimized to produce optimum RMS image at the edge of the field of view. The second order coefficients of the primary mirror and the secondary mirror are equal but they have opposite sign in order for them to cancel their on-axis aberrations. Next, a set of third order polynomial coefficients are optimized following the same principle. In this case the coefficients are equal and, therefore, introduce only minor image defects at the focal plane. In the final step coefficients of the axial fourth order polynomials are optimized in the same way as the coefficients of the second order polynomials.

Optimization for wide field of view designs is accomplished by adding additional second order Legendre polynomial to the axial profile of the secondary mirror only (or primary mirror only). The coefficient is optimized to produce minimum RMS image diameter at the optimal focal surface at the edge of the field of view and on-axis at the center of the field of view.

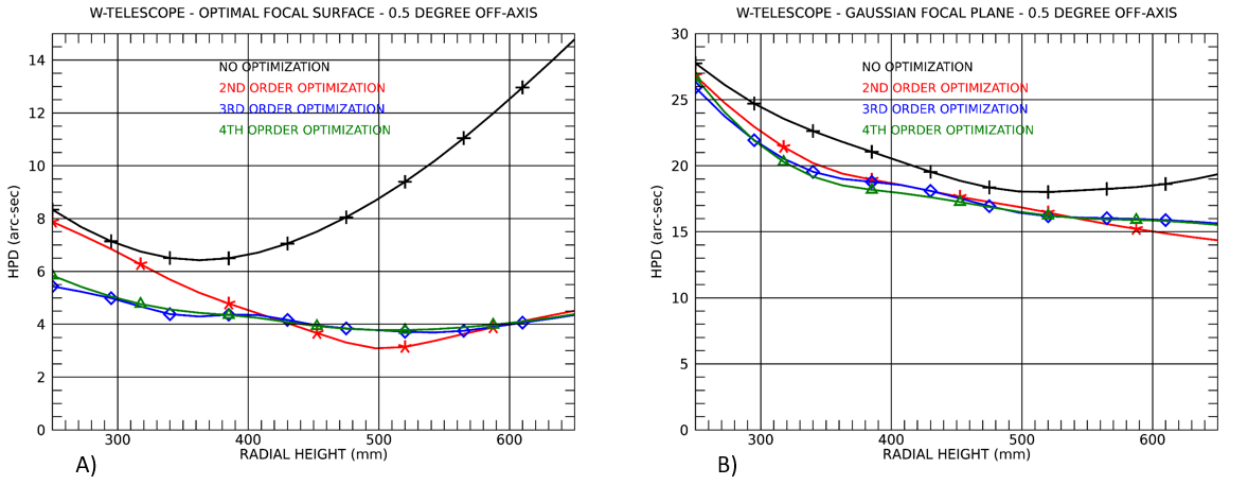

Figure 6. HPDs are plotted as a function of radial heights at A) the optimal focal surface and B) Gaussian focal plane at the edge of 0.5-degree field of view. Designs include W-telescopes (+), telescopes optimized for 2nd order coefficient (*), 2nd and 3rd order coefficients (◊), and 2nd, 3rd, and 4th order coefficients (Δ).

3.1. Optimized W-telescopes

As in HH-telescopes substantial improvement in image quality should be achieved when adding low order axial polynomials to the mirrors of W-telescopes. Figure 6A shows the HPD plotted as a function of radial heights of individual W-telescopes at the edge of 0.5-degree field of view at the optimal focal surface. The graph shows HPDs for the baseline W-telescopes, optimized W-telescopes for added second order polynomials, optimized W-telescopes for added second and third order polynomials, and optimized W-telescopes for added second, third, and fourth order polynomials. On-axis image quality for all these designs is still negligible. Optimized second order coefficients added to W-telescopes improve the optical performance substantially across the whole radial height range. Improvement increases when the radial heights of the mirrors are getting larger. Added third and fourth order coefficients further improve the HPD in the radius range from 250 mm to 420 mm. Figure 6B shows the optimized HPDs at the Gaussian focal plane. Only modest improvement is achieved when polynomials are added and the W-telescopes are optimized across the range of radial heights from 250 mm to 650 mm.

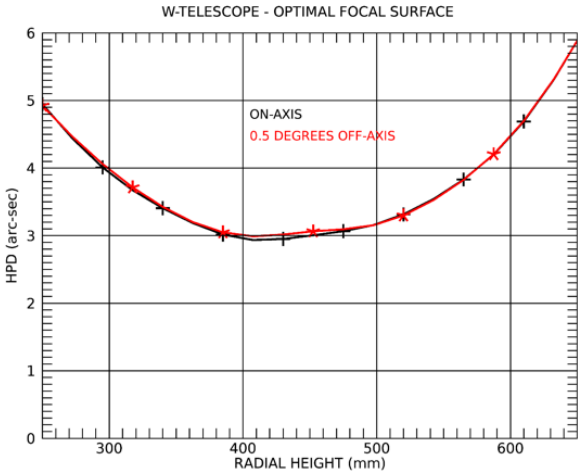

Figure 7. HPDs of individual optimized W-telescopes that have the same on-axis HPDs (+) and off-axis HPDs (*) at the optimal focal surface.

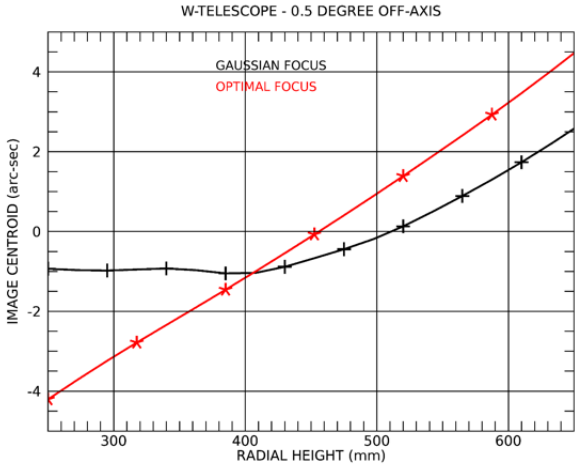

Figure 8. Image centroid locations of individual optimized W-telescopes at 0.5-degree locations at Gaussian focal plane (+) and optimal focal surface (*).

Figure 7 shows the optimized HPDs at the optimal focal surface when the W-telescopes are optimized for equal HPDs at the on-axis field point and 0.5-degree off-axis field point. HPDs range from 4.9 arc-sec to 5.9 arc-sec reaching a minimum of 3.0 arc-sec at radial height of about 400 mm.

Figure 8 shows the deviations of radial centroids at 0.5-degrees off-axis of the optimized W-telescopes from mean centroid values. The range of centroids vary about 8 arc-sec at the optimal focal surface. This range is the same as the range obtained and depicted for the HH-telescopes in Figure 5.

Axial location of optimal focal surface of optimized W-telescopes in the 250 mm to 650 mm radial height range is the same as shown in Figure 2 for the HH-telescopes. The field curvatures of these telescopes are the dominating aberration of the designs. Field curvatures increase sharply when the radial heights decrease.

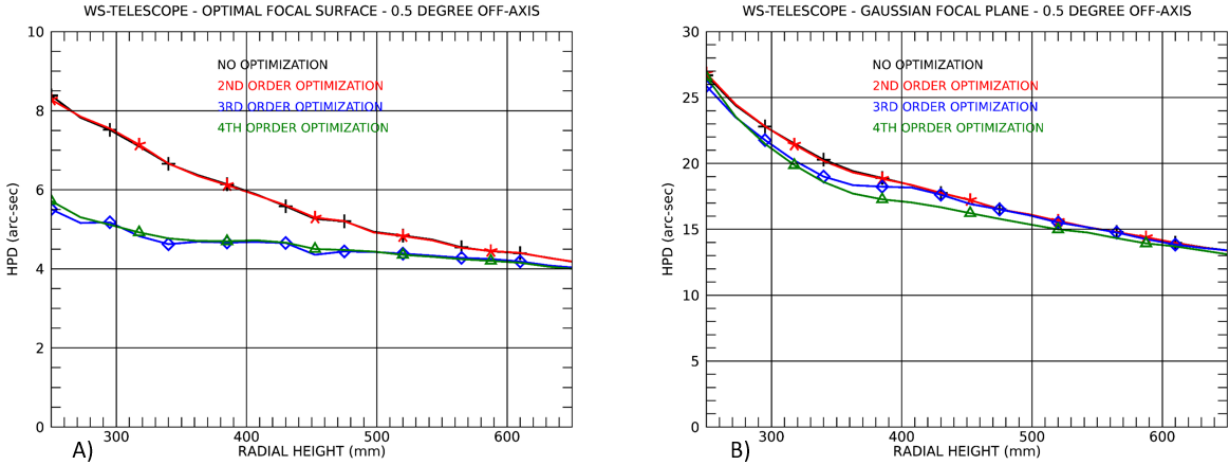

Figure 9. HPDs of WS-telescopes are shown as a function of radial heights at A) the optimal focal surface and B) at the Gaussian focal plane at the edge of 0.5-degree field of view. Designs include baseline WS-telescopes (+), telescopes optimized for 2nd order coefficient (*), 2nd and 3rd order coefficients (◊), and 2nd, 3rd, and 4th order coefficients (Δ).

3.2. Optimized WS-telescopes

WS-telescopes offer an excellent starting point for this optimization method since the telescopes are stigmatic and also they are free from third order coma aberration. Figure 9 plots the HPDs calculated 0.5-degrees off-axis as a function of radial heights at the optimal focal surface and Gaussian focal plane. Shown are optimizations of second order coefficients, second and third order coefficients, and second, third, and fourth order coefficients. As shown in Figure 9A, second order polynomial optimization does not improve the HPD at all. This is because added axial second order shapes tend to generate coma-type aberrations that do not exist in the WS-telescopes. Optimized fourth order additions to the surface profiles of the mirrors do not improve the HPDs for the same reason. Optimized third order additions improve substantially the performance of inner mirror pairs where the radial height of the mirrors are below about 600 mm. On-axis HPDs of these designs remain negligible.

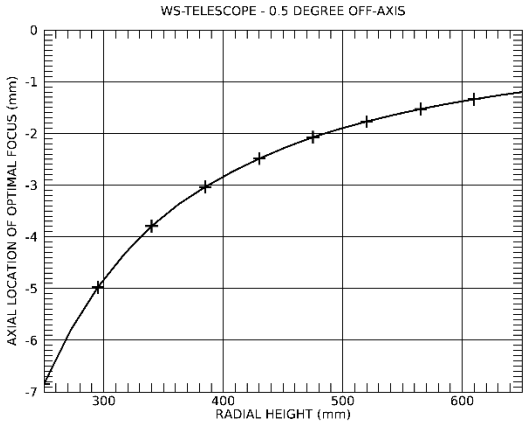

Figure 10. Axial location of optimal focus of WS-telescopes in radial height range from 250 mm to 650 mm.

At the Gaussian focal plane addition of the polynomials have only minor effect on the image quality. Only a few arc-second improvement is achieved in 250 mm to 400 mm radial height range when equal amounts of third order

and fourth order terms are added on the primary and secondary mirrors.

Figure 10 plots the axial location of optimal focal surface for the optimized WS-telescopes at the edge of 0.5-degree field of view. Field curvatures of the WS-telescopes form similar response as the W-telescopes and HH-telescopes illustrated in Figure 2. This is the dominating aberration in the WS-telescope systems.

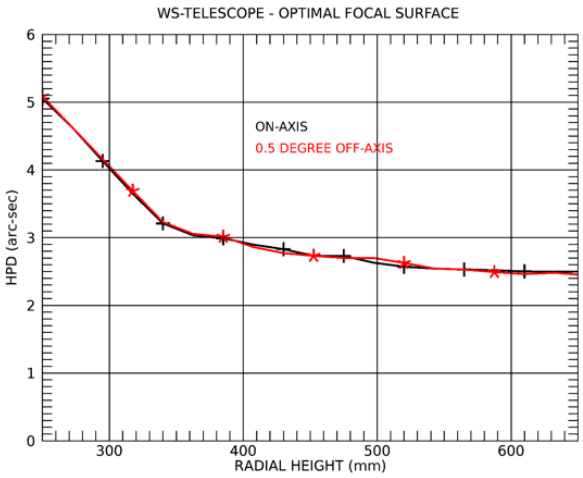

Figure 11. HPDs of the optimized WS-telescopes that have the same on-axis and off-axis performance at the optimal focal surface

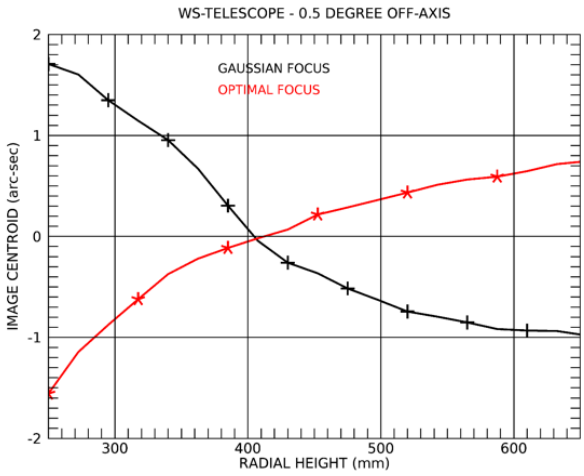

Figure 12. Image centroid locations for individual optimized WS-telescopes at 0.5-degree locations at Gaussian focal plane (+) and optimal focal surface (*).

WS-telescopes provide the best image HPDs when the designs are optimized to yield the same on-axis and off-axis image RMSD. Figure 11 plots the HPD as a function of the radial heights for the optimized WS-telescopes. Largest mirror pair provides the smallest HPD of about 2.5 arc-sec. The performance of WS-telescopes is significantly better than the performance of W-telescopes and HH-telescopes in 500-mm to 650-mm radial height range.

Figure 12 shows the deviation of the centroids of individual optimized telescopes from mean centroids at 0.5-degree off-axis location both at the Gaussian focal plane and optimal focal surface. Response of the WS-telescopes is significantly better than the deviation calculated for HH-telescopes and W-telescopes. Note that the deviation of the centroids at the optimal focal surface is calculated for individual telescopes. One would want to determine the

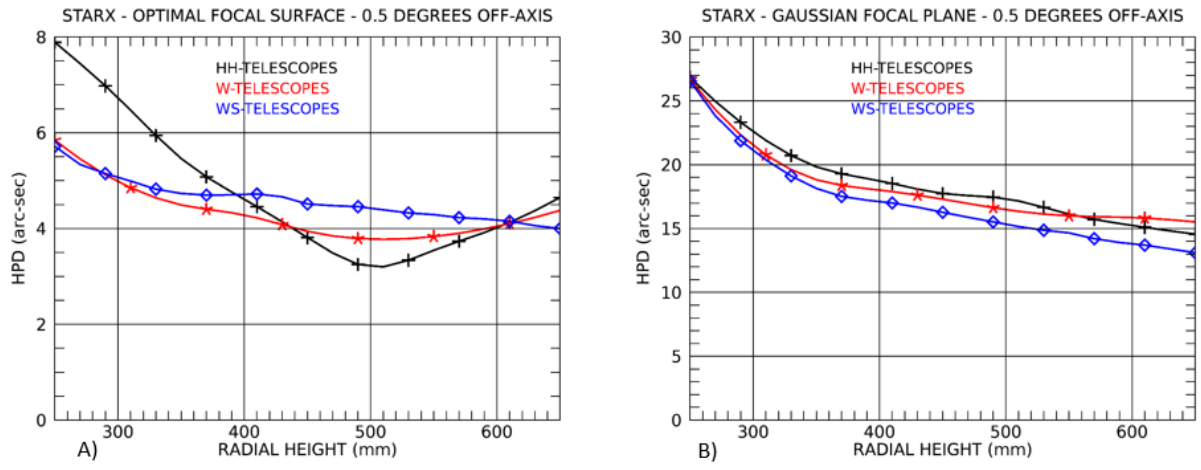

Figure 13. HPDs of HH-, W-, and WS-telescopes optimized at the edge of the field of view and at the optical axis are plotted in radial height range from 250 mm to 650 mm. Optical performance is shown A) at the optimal focal surface and B) at the Gaussian focal plane.

centroid deviations at the common optimal surface of the nested telescopes. This process would minimize the image errors caused by centroid deviations for the nested telescope systems.

4. COMPARISON OF OPTIMIZED TELESCOPES

At the optimal focal surface optical performances of optimized W- and WS- telescopes are remarkably similar for the telescopes designed for narrow field of view applications. Figure 13A compares the HPDs calculated in STARX radial height range. Interestingly at the edge of 0.5-degree field of view optimized W-telescopes outperform optimized WS-telescopes in wide radial height range 290 mm to 610 mm. Performance of HH-telescopes is excellent in 440 mm to 600 mm radial height range but poor below 400-mm radial heights. Note that HPDs of W-telescopes after only second order optimization are comparable to HPDs of HH-telescopes. On-axis performance of all the designs is still near perfect. At the Gaussian focal plane the performance of WS-telescopes is slightly better than the performance of W- and HH-telescopes and HPDs are about a factor of 3 larger. Figure 13B shows the results of the performance comparison.

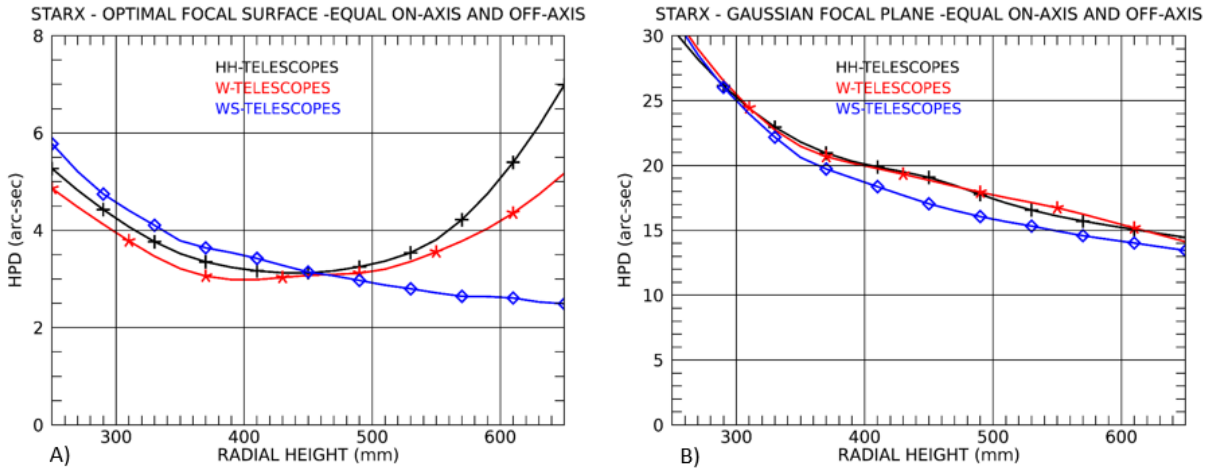

Figure 14. HPDs of HH-, W-, and WS-telescopes plotted as a function of radial heights at A) the optimal focal surface and B) at the Gaussian focal plane optimized for equal on-axis and off-axis performance

Performance of the HH-telescopes, optimized W-telescopes, and optimized WS-telescopes optimized for wide field of view (equal on-axis and off-axis HPDs) is shown in Figure 14A at the optimal focal surface and in Figure 14B at the Gaussian focal plane. At the optimal focal surface WS-telescopes provide superior performance at radial heights 460 mm or larger. In radial height range below 460 mm optimized W-telescopes outperforms HH-and optimized WS-telescopes. At the Gaussian focal plane HPDs of optimized WS-telescopes are slightly better especially in 400-mm to 650-mm radial height range.

5. OPTIMIZATION OF NESTED TELESCOPES

Optimization of nested x-ray telescopes is a complex process. Individual telescopes need to be optimized and a stack of nested telescopes needs to be optimized to provide optimum common on-axis and off-axis image quality. Also, grazing angles vary within the stack of nested telescopes leading to changes in geometric areas and reflectivities of individual telescopes. Effective areas of individual telescopes are therefore dependent on energy requirements of the telescope. The nested telescope can be optimized only for a single energy. From the telescope designs considered, WS-telescopes offer the best design options for wide field of view applications. If designed for equal on-axis and off-axis image quality, WS-telescopes are significantly better than W-telescopes and HH-telescopes. Also, the centroids of individual telescopes fall within smaller range. This should lead more compact images in the nested

telescope systems. Thus, an optimization method is presented here for the WS-telescopes only and for 1.0 keV energy requirement.

Large variation of the field curvatures of individual telescopes from inner mirror pair to outer mirror pair complicate the design of nested telescope systems. Individual telescopes cannot be optimized at their optimal focus locations in

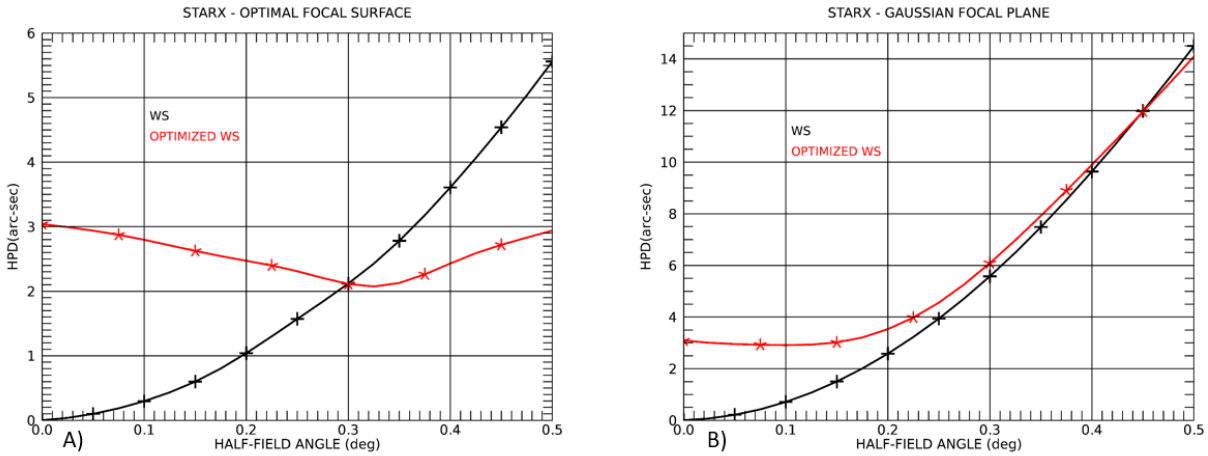

Figure 15. HPDs plotted as a function of half-field angle at A) the optimal focal surface and B) at the Gaussian focal plane. HPDs are calculated at 1.0 keV energy.

order to optimize a nested set of telescopes. In the optimization process nested WS-telescope [14, 15] is designed first. Optimization of individual telescopes is then done at the optimal focal surface of the nested WS-telescope. Second order axial sag terms of the secondary mirrors are varied to optimize RMSD of the telescopes. The optimized designs shown in this paper do not include second, third, or fourth order optimization terms added into the optimization in Sections 3.1 and 3.2.

Figure 15A shows the HPD of nested WS-telescope and optimized nested WS-telescope at the optimal focal surface. HPD of optimized nested WS-telescope is more uniform across the field of view due to the optimized sags of the secondary mirrors. HPD is 3.0 arc-sec or below across the 1.0-degree field of view reaching a minimum of 2.1 arc-sec about 0.32 degrees from the center of the field of view. Figure 15B plots the HPD at the Gaussian focal plane for the nested WS-telescope and optimized nested WS-telescope. At the Gaussian focal plane optimization provides just a minor improvement at narrow range of larger field angles at the expense of lost resolution in the image field near the center of the field of view. Figure 16 plots the half-field angle as a function of axial location of the optimal focus for nested WS-telescope and optimized nested WS-telescope. In the optimization process individual WS-telescopes were optimized at the edge of the field of view -1.42 mm from the focus of nested WS-telescope. This choice seem to make optimal focus locations slightly worse in 0.45 – 0.05 degree range and the curve tends to deviate slightly from second order shape.

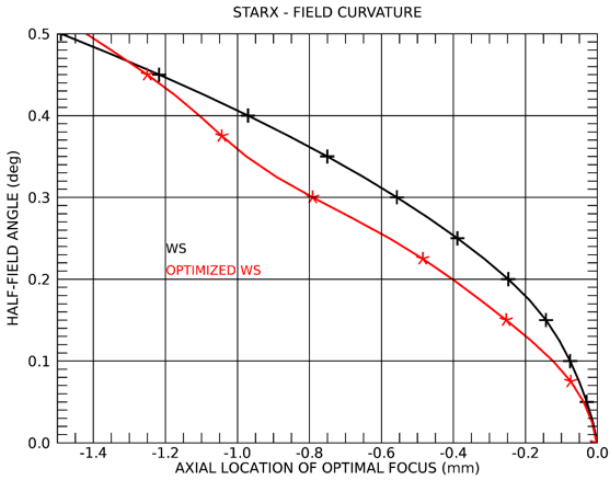

Figure 16. Half-field angle of nested WS-telescope and optimized WS-telescope plotted as a function of axial location of the optimized focus at 1.0 keV energy.

6. CONCLUSIONS

In the developed optimization methods axial low-order polynomials incorporated to the W-telescopes and WS-telescopes are used to optimize single off-axis field point or combination of on-axis and off-axis field points to produce optimum image quality for science application of interest. Similarly, on-axis and off-axis images of HH-telescopes can be optimized by varying the eccentricities of the mirrors. Substantial improvements in the image quality can be achieved at the optimal focal surface of the telescopes. At the Gaussian focal plane only modest improvements are attainable.

Off-axis image quality of W-telescopes can be significantly improved for narrow field of view applications. Added polynomials reshape the off-axis comatic images. They become more symmetric with respect to their centroids leading to substantial improvements in the HPDs or RMDs. In fact, at the optimal focal surface, HPDs of individual mirror pairs of STARX telescope outperform the optimized mirror pairs of WS-telescopes across large portion of radial height range of the individual telescopes. HH-telescopes can also be optimized to outperform optimized WS-telescopes over narrow range of radial heights. At the Gaussian focal plane improvements in optical performance of optimized W-telescopes, optimized WS-telescopes, and HH-telescopes are modest. Optimized WS-telescopes provide best performance across the radial height range.

Optimization of polynomials for equal on-axis and off-axis performance improve the performance substantially at the edge of the field of view at the expense of on-axis performance. At the optimal focal surface optimized WS-telescopes are superior in radial height range above 460 mm. Optimized W-telescopes provide slightly improved performance below 460-mm radial heights. At the Gaussian focal plane HPDs of optimized WS-telescopes are slightly smaller across the radial height range.

Varying field curvatures of individual telescopes from the inner shell pair to the outermost shell pair complicate the optimization process of nested telescopes. WS-telescopes are best suited for the optimization across the wide field of view because they provide the best on-axis and off-axis HPDs and centroid deviations of the individual telescopes from the nominal centroids. Optimization of second order sags of individual telescopes provides nested designs with performance at optimal focal surface about 3 arc-sec or below across a1.0 degree field of view. At the Gaussian focal plane performance of nested WS-telescope is significantly better near on-axis field points and slightly better close to the edge of the 1.0-degree field of view. Further improvements in the optical performance of nested telescopes are possible by adding axial third order terms on the primary and secondary mirrors. Also, axial locations of the individual mirror pairs could be optimized to better match the centroid locations of the images at the optimal focal surface.

7. ACKNOWLEDGEMENTS

This work has been financially supported by the Next Generation X-Ray Optics Project at Goddard Space Flight Center in Greenbelt, Maryland.

REFERENCES

[1] Peter M. Solly, Michael P. Biskach, Joseph Bonafede, Kai-Wing Chan, James R. Mazzarella, Ryan S. McClelland, Timo T. Saha, and William W. Zhang, “Structural analysis and testing of silicon x-ray mirror modules, “Proc. SPIE 11119-11 (2019).

[2] William W. Zhang, ”Next-generation astronomical x-ray optics: high-resolution, lightweight, and low-cost, Proc. SPIE, **11119**-6 (2019).

[3] Raul E. Riveros, Michael P. Biskach, Kim D. Allgood, John D. Kearney, Michal Hlinka, Ai Numata, William W. Zhang,” Fabrication of mono-crystalline silicon mirrors for x-ray telescopes , Proc. SPIE, 11119-7 (2019).

[4] Kai-Wing Chan, James R. Mazzarella, Timo T. Saha, William W. Zhang, Michael P. Biskach, Peter M. Solly, Raul E. Riveros, and Ai Numata, “Recent advances in the alignment of silicon mirrors for high-resolution x-ray optics, Proc. SPIE **11119**-10 (2019).

[5] H. Wolter, "Mirror Systems with Glancing Incidence as Image Producing Optics for X- Rays," Ann. Phys. 10, 94 (1952).

[6] L. P. Van Speybroeck and R.C. Chase, “Design parameters of paraboloid-hyperboloid telescopes for x-ray astronomy, Appl. Opt. **11**, 440-445 (1972).

[7] R. C. Chase and L. P. VanSpeybroeck, “Wolter-Schwarzschild telescopes for x-ray astronomy, “Appl. Opt., **12**, 1042-1044 (1973).

[8] Timo T. Saha, “General surface equations for glancing incidence telescopes, “Appl. Opt., **26**, 658-663 (1987).

[9] James E. Harvey, Andrey Krywonos, Patrick L. Thompson, and Timo T. Saha, ”Grazing incidence hyperboloid-hyperpoloid designs for wide-field x-ray imaging applications,”Appl. Opt., **40**, 136-144 (2001).

[10] Christopher J. Burrows, Richard Burg, and Riccardo Giacconi, “Ap.J., **392**, 760-765 (1992).

[11] Paolo Conconi, Sergio Campana, Gianpiero Tagliaferri, Giovanni Pareschi, Obertto Citterio, Vincenzo Cotroneo, Laure Proserpio, and Martha Civitani, “A wide field X-ray telescope for astronomical survey purposes: from theory to practice, “Mon. Not. R. Astron. Soc., **405**, 877-886 (2010).

[12] Ronald F. Elsner, Stephen L. O’Dell, Brian D. Ramsey, and Martin C. Weisskopf, “Methods of optimizing x-ray optical prescriptions for wide-field applications, “Proc. SPIE, **7732,** 77322L-77322L-14 (2010).

[13] Peter. W .A. Roming, John C. Liechty, David H. Sohn, Jared R. Shoemaker, David N. Burrows, Gordon P. Garmire, “Markov chain Monte Carlo algorithms for optimizing grazing incidence optics for wide-field x-ray survey imaging, “Proc. SPIE, **4496**, 146-153 (2002).

[14] Timo T. Saha, Ryan S. McClelland, and William W. Zhang, “Optical Design for a survey telescope, “Proc. SPIE **9144,** 914418-1-914418-12 (2014).

[15] Timo T. Saha, William W. Zhang, and Ryan S. McClelland, "Optical design of the STAR-X telescope," Proc. SPIE **10399**, 103990I (2017).

[16] P. Glenn, R.J. Noll and J.F. Osantowski, “Optical Surface Analysis Code (OSAC), “Proc. SPIE, **362**, 78(1982).

[17] Paul Glenn, “Set of orthonormal surface error descriptors for near-cylindrical optics, “Opt. Eng., **23**, 384 -390 (1984).